



## Copper(II) halide coordination complexes and salts of 3-halo-2-methylpyridines: Synthesis, structure and magnetism

Mahmoud Abdalrahman<sup>a</sup>, Christopher P. Landee<sup>b</sup>, Shane G. Telfer<sup>c</sup>, Mark M. Turnbull<sup>a,\*</sup>, Jan L. Wikaira<sup>d</sup>

<sup>a</sup> Carlson School of Chemistry and Biochemistry, Worcester, MA 01610, United States

<sup>b</sup> Dept. of Physics, Clark University, 950 Main St., Worcester, MA 01610, United States

<sup>c</sup> MacDiarmid Institute for Advanced Materials and Nanotechnology, Institute of Fundamental Sciences, Massey University, Palmerston North, New Zealand

<sup>d</sup> Dept. of Chemistry, University of Canterbury, Private Bag 4800, Christchurch, New Zealand

### ARTICLE INFO

#### Article history:

Available online 7 February 2012

Dedicated to Prof. Jon Zubieta

#### Keywords:

Copper halides  
Crystal structures  
Magnetic measurements  
Halopyridine complexes

### ABSTRACT

Two families of compounds have been prepared from the reaction of 3-*X'*-2-methylpyridine with  $\text{CuX}_2$  ( $X, X' = \text{Cl}, \text{Br}$ ) in the presence or absence of  $\text{HX}$ . Four salts,  $(3\text{-}X'\text{-2-methylpyridinium})_2\text{CuX}_4$  were prepared, three of which crystallize in the orthorhombic space group  $Pbcn$  while the fourth ( $X = \text{Br}$  and  $X' = \text{Cl}$ ) crystallizes in the monoclinic space group  $C2/c$ . All four neutral compounds of formula  $(3\text{-}X'\text{-2-methylpyridine})_2\text{CuX}_2$  crystallize in the space group  $P\bar{1}$ . Of these, three form weakly bridged chains via long  $\text{Cu}\cdots\text{X}$  contacts, while the fourth ( $X = X' = \text{Cl}$ ) forms centrosymmetric dimers. Most of the complexes exhibit only very weak antiferromagnetic interactions and can be modeled as weak uniform chains. Compound **4**,  $(3\text{-Cl-2-methylpyridinium})_2\text{CuBr}_4$ , shows behavior that models an isolated 2D-Heisenberg antiferromagnetic layer with  $J = -5.09(2)$  K, while compound **7**,  $(3\text{-Cl-2-methylpyridine})_2\text{CuCl}_2$ , crystallizes as a bichloride bridged centrosymmetric dimer with  $J = -29.31(6)$  K.

© 2012 Elsevier B.V. All rights reserved.

### 1. Introduction

The bulk magnetic properties of transition metal complexes are dependent upon chemical connectivity, local geometry, and non-bonding contacts between magnetic species in the crystalline lattice. We have been studying magneto-structural correlations in copper(II) halide coordination complexes and salts in an attempt to understand the factors that affect the magnetic superexchange pathways in the compounds and to derive quantitative structure/function relationships. There are two common superexchange pathways in cupric halides: bihalide bridges, where a pair of halide ions bridge a pair of  $\text{Cu(II)}$  ions, and the two-halide pathway ( $\text{Cu}\cdots\text{X}\cdots\text{Cu}$ ) where non-bonding overlaps between the halide ions mediate the magnetic exchange. In both cases, there are multiple bond lengths, angles, dihedral angles, geometric distortions, etc. that may contribute to the overall pathway [1]. Correlations between the magnetic properties and the structure of compounds have continually been drawn [2]. Given the large number of potential controlling factors, a similarly large number of compounds are necessary to provide the data needed to attempt any degree of quantitative correlation. To that end, we have been studying families of  $\text{Cu(II)}$  coordination complexes and salts of substituted pyridines with the general formulae  $(\text{AH})_2\text{CuX}_4$  or  $(\text{A})_2\text{CuX}_2$  where A is

the substituted pyridine which serves as an organic base or ligand, and X is bromide or chloride.

For both the salts and neutral complexes, the size, shape and location of substituents on the pyridine rings has a major effect on the crystal packing. Systems with magnetic interactions that form dimers [3], chains [4], ladders [5], layers [6] and three-dimensional systems [7] have all been isolated. We have recently reported work involving the complexes of  $\text{CuX}_2$  with 2-*X*-3-methylpyridine ( $X = \text{Cl}, \text{Br}$ ) where the magnetic behavior of the compounds was successfully fit to models for dimers or chains [8]. In the present work, the relative positions of the halogen and methyl group have been reversed and we report here the synthesis, structure, and magnetic behavior of the compounds  $(3\text{-}X'\text{-2-methylpyridinium})_2\text{CuX}_4$  (**1**,  $X = \text{Cl}, X' = \text{Br}$ ; **2**,  $X = X' = \text{Br}$ ; **3**,  $X = X' = \text{Cl}$ ; **4**,  $X = \text{Br}, X' = \text{Cl}$ ) and  $(3\text{-}X'\text{-2-methylpyridine})_2\text{CuX}_2$  (**5**,  $X = \text{Cl}, X' = \text{Br}$ ; **6**,  $X = X' = \text{Br}$ ; **7**,  $X = X' = \text{Cl}$ ; **8**,  $X = \text{Br}, X' = \text{Cl}$ ).

### 2. Experimental

3-Bromo-2-methylpyridine was purchased from AK Scientific, Inc. and 3-chloro-2-methylpyridine was purchased from Synchem OHG and used without further purification. Copper chloride, copper bromide, HCl and HBr were obtained from VWR and used without further purification. IR spectra were recorded on a Perkin Elmer Spectrum 100 spectrometer. Elemental analyses were carried out by Marine Science Institute, University of California, Santa Barbara, CA 93106, USA.

\* Corresponding author.

E-mail address: [mturnbull@clarku.edu](mailto:mturnbull@clarku.edu) (M.M. Turnbull).

### 2.1. Synthesis of bis(3-bromo-2-methylpyridinium) tetrachlorocuprate(II) (**1**)

A solution of 3-bromo-2-methylpyridine (0.300 g, 1.74 mmol) in 0.5 mL conc.  $\text{HCl}_{(\text{aq})}$  was added to a solution of copper chloride (0.117 g, 0.873 mmol) in 2.5 mL of conc.  $\text{HCl}_{(\text{aq})}$  with stirring. One mL of 6 M  $\text{HCl}_{(\text{aq})}$  was added. The resulting green solution was left to evaporate at room temperature. After several days, orange crystals were harvested by vacuum filtration, washed with 2-methyl-2-propanol, and allowed to air dry to give 0.158 g (26%). Further evaporation of the filtrate yielded an additional 0.109 g (17%). IR (KBr): 3250w, 3142w, 3082m, 3011sh, 2983m, 2886m, 2830s, 2796s, 2698s, 1608m, 1529s, 1459m, 809m, 666m  $\text{cm}^{-1}$ . *Anal. Calc.* for  $\text{C}_{12}\text{H}_{14}\text{N}_2\text{Cl}_4\text{CuBr}_2$ : C, 26.04; H, 2.55; N, 5.06. Found: C, 26.01; H, 2.61; N, 5.05%.

### 2.2. Synthesis of bis(3-bromo-2-methylpyridinium) tetrabromocuprate(II) (**2**)

A solution of 3-bromo-2-methylpyridine (0.207 g, 1.17 mmol) in 0.5 mL conc.  $\text{HBr}_{(\text{aq})}$  was added to a solution of copper bromide (0.130 g, 0.583 mmol) in 2 mL of conc.  $\text{HBr}_{(\text{aq})}$  with stirring. The resulting dark green solution was left to evaporate at room temperature (turning purple as the solution concentrated). After 2 months, dark purple crystals were harvested by vacuum filtration, washed with 2-methyl-2-propanol, and allowed to air dry to give 0.283 g (67%). IR (KBr): 3222w, 3137w, 3076m, 3006sh, 2978m, 2881m, 2839s, 2806s, 2688m, 1608m, 1524s, 1457m, 1346m, 797m, 664m  $\text{cm}^{-1}$ . *Anal. Calc.* for  $\text{C}_{12}\text{H}_{14}\text{N}_2\text{CuBr}_6$ : C, 19.60; H, 1.92; N, 3.81. Found: C, 19.32; H, 1.80; N, 3.61%.

### 2.3. Synthesis of bis(3-chloro-2-methylpyridinium) tetrachlorocuprate(II) (**3**)

A solution of 3-chloro-2-methylpyridine (0.100 g, 0.783 mmol) in 0.5 mL conc.  $\text{HCl}_{(\text{aq})}$  was added to a solution of copper chloride (0.0525 g, 0.392 mmol) in 1.5 mL of conc.  $\text{HCl}_{(\text{aq})}$  with stirring. The resulting green solution was left to evaporate at room temperature. After 3 weeks, orange crystals were harvested by vacuum filtration, washed with 2-methyl-2-propanol, and allowed to air dry to give 0.141 g (78%). IR (KBr): 3248w, 3160w, 3087m, 2987m, 2894m, 2832s, 2796s, 2701m, 1622m, 1533s, 1461m, 1384m, 1354m, 1293m, 1089m, 809s, 687s  $\text{cm}^{-1}$ . *Anal. Calc.* for  $\text{C}_{12}\text{H}_{14}\text{N}_2\text{Cl}_6\text{Cu}$ : C, 31.16; H, 3.05; N, 6.06. Found: C, 31.28; H, 2.92; N, 5.90%.

### 2.4. Synthesis of bis(3-chloro-2-methylpyridinium) tetrabromocuprate(II) (**4**)

A solution of 3-chloro-2-methylpyridine (0.206 g, 1.57 mmol) in 0.75 mL conc.  $\text{HBr}_{(\text{aq})}$  was added to a solution of copper bromide (0.175 g, 0.785 mmol) in 2.5 mL of conc.  $\text{HBr}_{(\text{aq})}$  with stirring. The resulting dark green solution was left to evaporate at room temperature (turning purple as the solution concentrated). After 2 months, dark purple crystals were harvested by vacuum filtration, washed with 2-methyl-2-propanol, and allowed to air dry to give 0.382 g (75%). IR (KBr): 3241w, 3156w, 3022m, 2989m, 2910m, 2846s, 2818s, 2699m, 1617s, 1531s, 1458w, 1386m, 1352m, 1287m, 1088m, 782s, 681m  $\text{cm}^{-1}$ . *Anal. Calc.* for  $\text{C}_{12}\text{H}_{14}\text{N}_2\text{Cl}_6\text{Cu}$ : C, 31.16; H, 3.05; N, 6.06. Found: C, 31.28; H, 2.92; N, 5.90%.

### 2.5. Synthesis of bis(3-bromo-2-methylpyridine)dichlorocuprate(II) (**5**)

A solution of 3-bromo-2-methylpyridine (0.150 g, 0.872 mmol) in 1 mL of absolute ethanol was added to a solution of copper chloride (0.060 g, 0.446 mmol) in 4 mL of absolute ethanol. The resulting dark green solution was left to evaporate at room temperature.

Blue crystals were harvested by vacuum filtration, washed with 2-methyl-2-propanol, and allowed to air dry to give 0.056 g (13%). Recrystallization from dichloromethane gave X-ray quality crystals. IR (KBr): 3060w, 3016w, 1590m, 1435s, 1060s, 806s, 710m  $\text{cm}^{-1}$ . *Anal. Calc.* for  $\text{C}_{12}\text{H}_{12}\text{N}_2\text{Cl}_2\text{CuBr}_2$ : C, 29.99; H, 2.52; N, 5.83. Found: C, 30.10; H, 2.59; N, 5.79%.

### 2.6. Synthesis of bis(3-bromo-2-methylpyridine)dibromocuprate(II) (**6**)

A solution of 3-bromo-2-methylpyridine (0.201 g, 1.17 mmol) in 0.5 mL of absolute ethanol was added to a solution of copper bromide (0.129 g, 0.578 mmol) in 2.5 mL of absolute ethanol. A dark green ppt. formed almost immediately. The powder was harvested by vacuum filtration, washed with 2-methyl-2-propanol, and allowed to air dry to give 0.252 g (77%). Slow evaporation of the filtrate gave X-ray quality crystals. IR (KBr): 3067w, 3011w, 1591m, 1459s, 1432s, 1062s, 802s, 708m  $\text{cm}^{-1}$ . *Anal. Calc.* for  $\text{C}_{12}\text{H}_{12}\text{N}_2\text{CuBr}_4$ : C, 25.22; H, 2.12; N, 4.90. Found: C, 25.30; H, 2.19; N, 4.80%.

### 2.7. Synthesis of bis(3-chloro-2-methylpyridine)dichlorocuprate(II) (**7**)

A solution of 3-chloro-2-methylpyridine (0.201 g, 1.58 mmol) in 0.5 mL of absolute ethanol was added to a solution of copper chloride (0.106 g, 0.791 mmol) in 2 mL of absolute ethanol. A dark blue ppt. formed almost immediately. The powder was harvested by vacuum filtration, washed with 2-methyl-2-propanol, and allowed to air dry to give 0.238 g (77%). Recrystallization from 1-propanol gave X-ray quality crystals. IR (KBr): 3059m, 3013w, 1589m, 1438s, 1086s, 1073s, 807s, 709s  $\text{cm}^{-1}$ . *Anal. Calc.* for  $\text{C}_{12}\text{H}_{12}\text{N}_2\text{Cl}_4\text{Cu}$ : C, 36.99; H, 3.10; N, 7.19. Found: C, 36.28; H, 2.81; N, 6.79%.

### 2.8. Synthesis of bis(3-chloro-2-methylpyridine)dibromocuprate(II) (**8**)

A solution of 3-chloro-2-methylpyridine (0.202 g, 1.59 mmol) in 0.75 mL of absolute ethanol was added to a solution of copper bromide (0.176 g, 0.789 mmol) in 4 mL of absolute ethanol. A dark green ppt. formed almost immediately. The powder was harvested by vacuum filtration, washed with 2-methyl-2-propanol, and allowed to air dry to give 0.241 g (64%). Recrystallization from absolute ethanol gave X-ray quality crystals. IR (KBr): 3060w, 3016w, 1590m, 1435s, 1060s, 806s, 710m  $\text{cm}^{-1}$ . *Anal. Calc.* for  $\text{C}_{12}\text{H}_{12}\text{N}_2\text{Cl}_2\text{CuBr}_2$ : C, 29.99; H, 2.52; N, 5.83. Found: C, 29.40; H, 2.53; N, 5.57%.

### 2.9. X-ray data collection

In several cases, X-ray quality crystals formed spontaneously from the reaction mixture. All compounds could be recrystallized from absolute ethanol, or 1-propanol. Data collections for compounds **1**, **2** and **5** were carried out on a Bruker Apex II diffractometer utilizing Mo  $\text{K}\alpha$  radiation ( $\lambda = 0.71073 \text{ \AA}$ ) and a graphite monochromator. The data collection, cell refinement, and data reduction were performed using SHELXTL [9]. Data collections for compounds **3**, **4**, **6**, **7** and **8** were carried out with a Rigaku–Spider X-ray diffractometer employing Cu  $\text{K}\alpha$  radiation ( $\lambda = 1.5418 \text{ \AA}$ ) and a Rigaku MM007 microfocus rotating-anode generator focused with high-flux Osmic multilayer mirror optics and a curved image-plate detector. CRYSTALCLEAR [10] was utilized for data collection and FSPROCESS in PROCESS-AUTO [11] for cell refinement and data reduction. The structures were solved by direct methods and refined via least-squares analysis using SHELX97-2 [12]. All non-hydrogen atoms were refined anisotropically. Hydrogen atoms bonded to N atoms were located in the difference maps and their positions refined using fixed isotropic  $U$  values. Hydrogen atoms bonded to C atoms were refined using a riding model with fixed

isotropic  $U$  values. Crystallographic data may be found in Tables 1a and 1b. Selected bond lengths and angles are given in Table 2. Hydrogen bonds are given in Table 3.

### 2.10. Magnetic susceptibility data collection

Magnetic data were collected using a Quantum Design MPMS-XL SQUID magnetometer. Finely ground samples of the crystals were packed in gelatin capsules. The moment was measured as a function of field from 0 to 50 kOe at 1.8 K. Several data points were also collected as the field was brought back to 0 kOe to check for hysteresis; no hysteresis was observed. In all cases the moment was linear as a function of field to at least 3 kOe. Temperature dependant magnetization data was collected in a 1 kOe field from 1.8 to 310 K. The contribution from the sample holder was measured separately and subtracted from all data sets. A temperature independent paramagnetism (TIP) correction of  $60 \times 10^{-6}$  for copper (II) was applied. Diamagnetic corrections were estimated from Pascal's constants [13].

## 3. Results

### 3.1. Synthesis

Reaction of  $\text{CuX}_2$  with 3- $X'$ -2-methylpyridine in aqueous HX gave crystals of (3- $X'$ -2-methylpyridinium) $_2\text{CuX}_4$  in 17–78% yield (see Scheme 1).

Similarly, reaction of  $\text{CuX}_2$  with 3- $X'$ -2-methylpyridine in alcohol (ethanol or 1-propanol), gave the corresponding neutral complexes (3- $X'$ -2-methylpyridinium) $_2\text{CuX}_2$  in 13 to 77% yield (see Scheme 2).

### 3.2. Crystal structure analysis - salts

Compounds **1–3** crystallize in the orthorhombic space group  $Pb\bar{c}n$ . Fig. 1 shows the molecular unit of **1**. The Cu(II) ions sit on a crystallographic twofold axis and the  $\text{CuCl}_4^{2-}$  ion is a flattened

tetrahedron with a mean trans angle of  $131.11(3)^\circ$  [14] and a mean Cu–Cl bond length of  $2.255(1) \text{ \AA}$ .

The 3-bromo-2-methylpyridinium ions are hydrogen bonded to the tetrachlorocuprates via  $\text{N1-H1} \cdots \text{Cl1A}$  (see Table 3) and the pyridinium rings are planar as expected (mean deviation of constituent atoms =  $0.0067 \text{ \AA}$ ). The compound crystallizes in layers parallel to the A-face of the crystal in an ABBABB pattern, with layers of  $\text{CuCl}_4^{2-}$  anions separated by double layers of pyridinium cations (see Fig. 2a). This results in weak  $\pi$ -stacking interactions between pyridinium ions in adjacent layers (see Fig. 2b). The interplanar distance between the mean plane of one pyridinium ring and the centroid of the second ring is  $3.303(2) \text{ \AA}$  and the angle between the rings is  $5.3(1)^\circ$ . The distance between the ring centroids is  $3.682(2) \text{ \AA}$  and the slip angle is  $26.2(1)^\circ$ .

The  $\text{CuCl}_4^{2-}$  ions pack into chains parallel to the  $c$ -axis with pairs of short, symmetry equivalent  $\text{Cl} \cdots \text{Cl}$  contacts (Fig. 3, Table 4). These contacts provide a potential magnetic superexchange path. The chains are well isolated; the shortest interchain  $\text{Cl} \cdots \text{Cl}$  contacts are greater than  $5.2 \text{ \AA}$ .

Compound **2** (Fig. 4) is isomorphous with **1**. Again, the Cu(II) ions sit on a crystallographic twofold axis, however the  $\text{CuBr}_4^{2-}$  ion is slightly less flattened with a mean trans angle of  $129.55(4)^\circ$  and a mean Cu–Br bond length of  $2.385(1) \text{ \AA}$ . The pyridinium rings are again flat (mean deviation =  $0.0086 \text{ \AA}$ ). Compound **2** packs in the same fashion as **1**, with weak  $\pi$ -stacking interactions between pairs of 3-bromo-2-methylpyridinium ions, the angle between the ring planes being  $4.3(1)^\circ$ . The mean distance between planes is  $3.354(1) \text{ \AA}$ , slightly larger than in **1**, the distance between the ring centroids is  $3.755(2) \text{ \AA}$  and the slip angle is  $26.7(1)^\circ$ . The  $\text{CuBr}_4^{2-}$  units are linked into chains similar to that seen in **1** (see Table 4) with a slightly shorter halide  $\cdots$  halide distance.

Compound **3** is also isomorphous with **1** and **2** (see Fig. 5). The average Cu–Cl bond length is  $2.256(6) \text{ \AA}$  and the mean trans angle at the Cu(II) ion is  $131.2(1)^\circ$ , comparable to that seen in **1**. The pyridinium rings are flat (mean deviation =  $0.0054 \text{ \AA}$ ) with similar  $\pi$ -stacking interactions (angle between adjacent rings =  $4.1(1)^\circ$ ; interplanar distance =  $3.299(2) \text{ \AA}$ ; centroid distance =  $3.635(2) \text{ \AA}$ ; slip angle =  $24.4(1)^\circ$ ). Halide-halide contacts again link the

**Table 1a**  
X-ray data for compounds **1–4**.

Compound	<b>1</b>	<b>2</b>	<b>3</b>	<b>4</b>
Empirical formula	$\text{C}_{12}\text{H}_{14}\text{N}_2\text{Cl}_4\text{CuBr}_2$	$\text{C}_{12}\text{H}_{14}\text{N}_2\text{CuBr}_6$	$\text{C}_{12}\text{H}_{14}\text{N}_2\text{Cl}_6\text{Cu}$	$\text{C}_{12}\text{H}_{14}\text{N}_2\text{Cl}_2\text{CuBr}_4$
Molecular weight	551.41	729.25	462.49	640.33
$T$ (K)	113(2)	113(2)	153(2)	148(2)
Crystal system	orthorhombic	orthorhombic	orthorhombic	monoclinic
Space group	$Pb\bar{c}n$	$Pb\bar{c}n$	$Pb\bar{c}n$	$C2/c$
$a$ (Å)	12.7218(4)	12.9660(4)	12.6158(9)	13.2998(4)
$b$ (Å)	12.5397(4)	12.8646(4)	12.4437(5)	7.8943(2)
$c$ (Å)	11.2824(3)	11.5493(3)	11.2823(2)	18.5364(15)
$\beta$ (°)				103.874(8)
$V$ (Å) <sup>3</sup>	1799.85(9)	1926.45(10)	1771.18(15)	1889.41(17)
$Z$	4	4	4	4
$D_{\text{calc}}$ (Mg/m <sup>3</sup> )	2.035	2.514	1.734	2.251
Absorption coefficient (mm <sup>-1</sup> )	6.240	13.572	10.015	14.096
$F(000)$	1068	1356	924	1212
Crystal size (mm)	$0.70 \times 0.63 \times 0.30$	$0.60 \times 0.24 \times 0.17$	$0.24 \times 0.18 \times 0.04$	$0.6 \times 0.4 \times 0.25$
$\theta_{\text{min}}$ , $\theta_{\text{max}}$ (°)	2.91, 30.0	2.84–25.02	7.02–72.01	6.57–71.84
Index ranges	$-18 \leq h \leq 18$ $-18 \leq k \leq 18$ $-16 \leq l \leq 16$	$-15 \leq h \leq 15$ $-15 \leq k \leq 15$ $-13 \leq l \leq 13$	$-15 \leq h \leq 15$ $-15 \leq k \leq 12$ $-13 \leq l \leq 13$	$-15 \leq h \leq 16$ $-8 \leq k \leq 9$ $-22 \leq l \leq 21$
Reflections collected	44212	33394	12778	6935
Independent reflections	2623 [R(int) = 0.0478]	1700 [R(int) = 0.0641]	1726 [R(int) = 0.0316]	1797
Maximum/minimum transaction factors	0.2561/0.0972	0.2062/0.0451	0.6901/0.1973	1.0/0.61
Restraints/parameters	0/100	0/100	0/100	0/102
Final $R_1/wR_2$ [ $I > 2\sigma(I)$ ]	0.0206/0.0496	0.0201/0.0468	0.0239/0.0606	0.0306/0.0779
Goodness-of-fit (GOF) on $F^2$	1.030	1.093	1.205	1.183
Largest peak/hole (e <sup>-</sup> Å <sup>-3</sup> )	0.677/−0.392	0.612 and −0.496	0.397 and −0.393	0.714 and −0.552

**Table 1b**  
X-ray data for compounds 5–8.

Compound	5	6	7	8
Empirical formula	C <sub>12</sub> H <sub>12</sub> N <sub>2</sub> Cl <sub>2</sub> CuBr <sub>2</sub>	C <sub>12</sub> H <sub>12</sub> N <sub>2</sub> CuBr <sub>4</sub>	C <sub>12</sub> H <sub>12</sub> N <sub>2</sub> Cl <sub>4</sub> Cu	C <sub>12</sub> H <sub>12</sub> N <sub>2</sub> Cl <sub>2</sub> CuBr <sub>2</sub>
Molecular weight	478.50	567.40	389.58	478.50
T (K)	113(2)	153(2)	153(2)	153(2)
Crystal system	triclinic	triclinic	triclinic	triclinic
Space group	P1	P1	P1	P1
a (Å)	4.9557(2)	5.4616(2)	8.4573(2)	5.56120(10)
b (Å)	8.0111(4)	7.6573(2)	9.7618(2)	7.5374(2)
c (Å)	10.1482(5)	10.1865(7)	10.3933(7)	9.9611(7)
α (°)	92.389(3)	96.046(7)	64.301(4)	98.418(7)
β (°)	94.321(3)	92.495(7)	88.062(6)	92.143(7)
γ (°)	105.862(3)	106.966(7)	75.569(5)	107.561(8)
V (Å <sup>3</sup> )	385.63(3)	403.97(3)	746.07(6)	392.32(3)
Z	1	1	2	1
D <sub>calc</sub> (Mg/m <sup>3</sup> )	2.060	2.332	1.734	2.025
Absorption coefficient (mm <sup>-1</sup> )	6.929	13.393	8.541	10.956
F(000)	231	267	390	231
Crystal size (mm)	0.70 × 0.33 × 0.16	0.30 × 0.20 × 0.15	0.30 × 0.22 × 0.08	0.76 × 0.60 × 0.25
θ <sub>min</sub> , θ <sub>max</sub> (°)	4.04, 54.68	7.05, 60.00	6.86, 61.75	7.08, 60.08
Index ranges	−6 ≤ h ≤ 5 −10 ≤ k ≤ 10 −13 ≤ l ≤ 13	−6 ≤ h ≤ 5 −8 ≤ k ≤ 8 −11 ≤ l ≤ 11	−9 ≤ h ≤ 9 −11 ≤ k ≤ 9 −11 ≤ l ≤ 11	−6 ≤ h ≤ 6 −8 ≤ k ≤ 8 −10 ≤ l ≤ 11
Reflections collected	7844	4917	13029	4754
Independent reflections	1740 [R(int) = 0.0381]	1173 [R(int) = 0.0551]	2234 [R(int) = 0.0295]	1147 [R(int) = 0.1011]
Maximum/minimum transaction factors	0.4036/0.0853	0.2386/0.1078	1.0/0.64	0.1704 and 0.0440
Restraints/parameters	0/89	0/89	0/174	0/89
Final R <sub>1</sub> /wR <sub>2</sub> [I > 2σ(I)]	0.0329/0.0812	0.0490/0.1276	0.0306/0.0819	0.0585/0.1480
Goodness-of-fit (GOF) on F <sup>2</sup>	1.094	1.104	1.037	1.066
Largest peak/hole (e <sup>-</sup> Å <sup>-3</sup> ) <sup>a</sup>	1.248/−0.823	1.688/−1.052	0.479/−0.606	0.965/−1.079

<sup>a</sup> Largest peaks and holes all found near halide ions.**Table 2**  
Bond lengths (Å) and angles (°) for 1–8.

Bond Lengths	1	2	3	4	5	6	7	8
Cu1–X1	2.2796(4)	2.4054(6)	2.2840(6)	2.4073(6)	2.2532(10)	2.4071(8)	2.3098(8)	2.3980(7)
Cu1–X2	2.2277(4)	2.3645(5)	2.2289(6)	2.3640(6)			2.2547(9)	
Cu1–X1A							2.7274(9)	
Cu1–N1					2.010(3)	1.999(6)	2.048(2)	1.995(7)
Cu1–N11							2.059(2)	
N1–C2/N11–C12	1.345(2)	1.340(6)	1.341(3)	1.346(6)	1.350(5)	1.326(9)	1.345(4)/1.349(4)	1.324(10)
N1–C6/N11–C16	1.345(2)	1.342(6)	1.341(3)	1.333(7)	1.338(5)	1.346(11)	1.347(4)/1.337(4)	1.343(8)
C2–C7/C12–C17	1.488(2)	1.487(6)	1.485	1.495(7)	1.488(5)	1.499(12)	1.492(5)/1.489(5)	1.477(9)
C3–X3/C13–X13	1.8813(18)	1.878(5)	1.730(3)	1.723(4)	1.896(4)	1.901(8)	1.742(3)/1.741(3)	1.739(9)
N1–H1	0.91(2)	0.81(5)	0.86(3)	0.77(5)				
Bond Angles								
X1–Cu–X2	99.742(16)	100.285(15)	99.65(2)	99.699(19)			100.46(3)	
X1–Cu–X1A	127.05(3)	126.31(4)	126.67(4)	123.33(4)			92.41(3)	
X1–Cu–X2A	99.833(15)	100.550(16)	99.76(2)	100.141(18)				
X2–Cu–X2A	135.17(3)	132.79(4)	135.88(4)	137.44(5)				
X1A–Cu–Cl2							171.92(3)	
X1–Cu–N1					90.23(9)	90.21(18)	94.27(8)	90.19(16)
N1–Cu–N11							171.14(11)	
C2–N1–C6/C12–N11–C16	124.28(15)	124.8(4)	124.4(2)	124.6(4)	121.1(3)	121.4(7)	119.8(3)/119.8(3)	121.6(7)

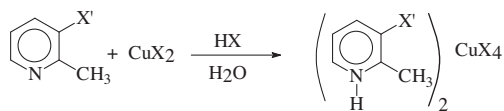
**Table 3**  
Hydrogen bonding for compounds 1–4.

Compound	D–H...A	d(D–H)	d(H...A)	d(D...A)	<(DHA)	Symm. op.
1	N(1)–H(1)...Cl(1)#1	0.91(2)	2.18(2)	3.0861(15)	174(2)	#1 –x, y, z + 5/2
2	N(1)–H(1)...Br(1)	0.81(5)	2.46(5)	3.237(4)	161(5)	
3	N(1)–H(1)...Cl1#2	0.86(3)	2.22(3)	3.076(2)	170(3)	#2 –x + 0.5, –y + 0.5, z + 0.5
4	N(1)–H(1)...Br(1)	0.77(5)	2.48(5)	3.251(4)	177(4)	

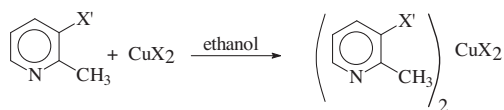
tetrahalocuprate units into chains (see Table 4), but with the longest X...X separation of compounds 1–3.

Compound 4 is unique among the salts and crystallizes in the monoclinic space group C2/c. Fig. 6 shows the molecular unit of 4. As was the case for 1–3, the Cu(II) ions sits on a crystallographic

twofold axis and the CuBr<sub>4</sub><sup>2-</sup> ion is a flattened tetrahedron with a mean trans angle of 130.4(1)° and a mean Cu–Br bond length of 2.386(1) Å. Unlike the pyridinium rings in 1–3, those of 4 are nearly perpendicular with an angle of 75.5(1)° between their mean planes.



**Scheme 1.** Preparation of salts (**1**, X = Cl, X' = Br; **2**, X = X' = Br; **3**, X = X' = Cl; **4**, X = Br, X' = Cl).



**Scheme 2.** Preparation of neutral complexes (**5**, X = Cl, X' = Br; **6**, X = X' = Br; **7**, X = X' = Cl; **8**, X = Br, X' = Cl).

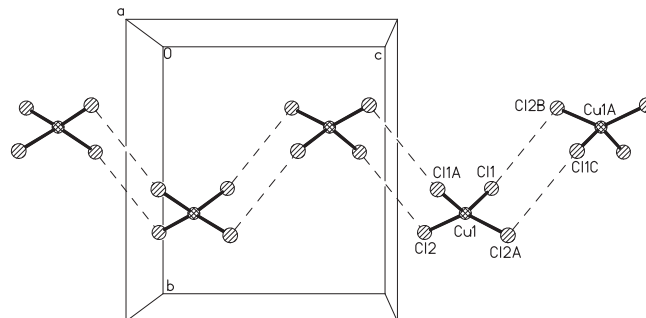


**Fig. 3.** Chain structure of **1** formed by short intermolecular Cu–Cl contacts parallel to the *c*-axis. Viewed parallel to the *a*-axis.

contacts [ $d_{\text{Br}2 \cdots \text{Cl}3\text{A}} = 3.591(3) \text{ \AA}$ ,  $\angle_{\text{Cu}1-\text{Br}2 \cdots \text{Cl}3\text{A}} = 164.7(2)^\circ$ ] are within the sum of their van der Waals radii.

### 3.3. Crystal structure analysis – neutral complexes

Complexes **5–8** have the general formula  $\text{Cu}_2\text{X}_2$  and crystallize in the triclinic space group *P*1. For compounds **5**, **6** and **8**, the Cu(II) ion is sited on a crystallographic inversion center. The molecular unit of **5** is shown in Fig. 10. All trans angles are  $180^\circ$  as required by symmetry and the N1–Cu–Cl1 angle is  $90.23(9)^\circ$ , making the complex nearly square planar.

The pyridinium ring is planar (mean deviation =  $0.0074 \text{ \AA}$ ), and tilted slightly off linear to the Cu1–N1 bond ( $<6.7(1)^\circ$ ) to the N1 $\cdots$ C4 vector). The ring is canted relative to the Cu(II) coordination plane ( $72.1(1)^\circ$ ). Adjacent molecular units are linked into chains by long Cu $\cdots$ Cl contacts parallel to the *a*-axis forming the bihalide bridge seen commonly in  $\text{Cu}_2\text{X}_2$  complexes (see Fig. 11 and Table 5), providing a potential magnetic superexchange pathway. The shortest chloride $\cdots$ chloride contact distance between chains is greater than  $8 \text{ \AA}$ , suggesting that the chains should be magnetically well isolated.

Although there are no close Cl $\cdots$ Cl contacts between chains, there are halogen–halide contacts which link the chains molecular units together (Fig. 12a) parallel to the *c*-axis, forming layers parallel to the B-face of the crystal (Fig. 12b). The Br3 $\cdots$ Cl1b distance is  $3.558(1) \text{ \AA}$ , while the C3–Br3 $\cdots$ Cl1b angle is  $157.0(2)^\circ$  and the Br3 $\cdots$ Cl1b–Cu1a angle is  $126.8(2)^\circ$ . These are typical for such halogen–halide contacts where the angle about the organic halogen (Br3) is nearer to  $180^\circ$  and the angle about the halide ion is nearer to  $90^\circ$  [15].

Compound **6** is isostructural with **5** and the molecular unit is shown in Fig. 13a. The N1–Cu–Br1 angle is  $90.21(18)^\circ$ , once again nearly square planar, and the pyridinium ring is again planar

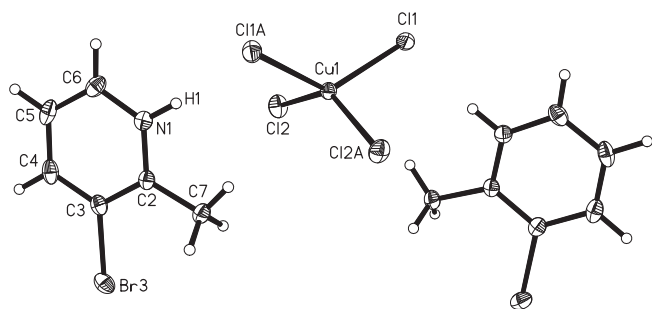


**Fig. 1.** Thermal ellipsoid plot of the molecular unit of **1** showing 50% probability ellipsoids. Only atoms in the asymmetric unit, the copper coordination sphere, and hydrogen atoms whose positions were refined are labeled.

The compound packs in layers parallel to the *ab*-face of the crystal. A similar ABBABB pattern forms with sheets of  $\text{CuBr}_4^{2-}$  ions separated by double layers of the organic cations (Fig. 7).

The layers of  $\text{CuBr}_4^{2-}$  ions map onto a square lattice with each  $\text{CuBr}_4^{2-}$  ion having four identical nearest neighbors (as a result of the C-centering) via short Br $\cdots$ Br contacts of  $4.18 \text{ \AA}$  (Fig. 8a). The next shortest Br $\cdots$ Br contact distance within a layer is greater than  $6.6 \text{ \AA}$ , making any secondary interactions within the layers negligible. Adjacent layers of  $\text{CuBr}_4^{2-}$  ions are not stacked directly above each other, but offset parallel to the *a*-axis (see Fig. 8b). As a result, the closest Br $\cdots$ Br contacts between layers are  $5.664(1) \text{ \AA}$ , significantly longer than the intraplane distance. The three dimensional structure is stabilized by hydrogen bonds (Table 3) and short halogen–halogen and halogen–halide contacts (see Fig. 9) which run parallel to the *ac*-face diagonal. Both the Cl $\cdots$ Cl contacts [ $d_{\text{Cl}3 \cdots \text{Cl}3\text{A}} = 3.547(3) \text{ \AA}$ ,  $\angle_{\text{C}3-\text{Cl}3 \cdots \text{Cl}3\text{A}} = 101.3(2)^\circ$ ] and the Cl $\cdots$ Br

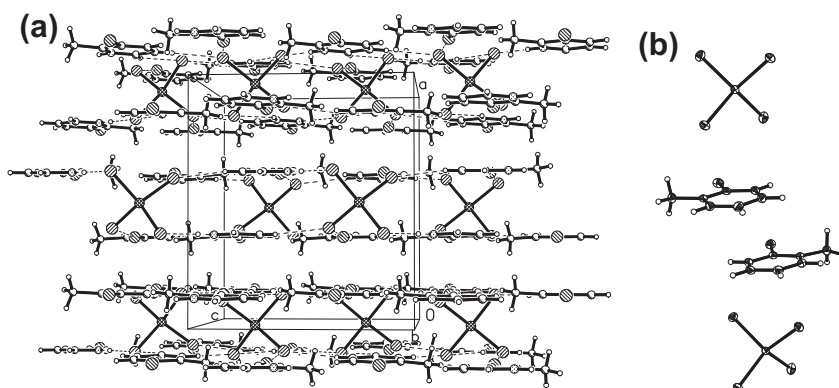


**Fig. 2.** (a) Packing diagram of **1** viewed parallel to the *b*-axis. Dotted lines represent hydrogen bonds. (b) ABBABB stacking of the  $\text{CuCl}_4^{2-}$  and pyridinium ion layers.

**Table 4**  
Halide–halide contacts for compounds 1–4.

Compound	$d_{X \dots X}$	$\langle \text{Cu1}-\text{X1} \dots \text{X2B} \rangle$	$\langle \text{X1} \dots \text{X2B}-\text{Cu1A} \rangle$	$\langle \text{Cu1}-\text{X1} \dots \text{X2B}-\text{Cu1A} \rangle$
1	4.403	130.5	101.3	44.4
2	4.395	131.1	99.7	67.1
3	4.430	130.7	101.2	66.7
4	4.181	156.7	122.2	16.5

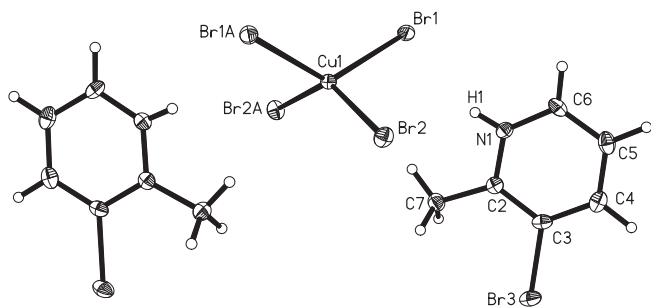


**Fig. 4.** Thermal ellipsoid plot of the molecular unit of **2** showing 50% probability ellipsoids. Only atoms in the asymmetric unit, the copper coordination plane, and hydrogen atoms whose positions were refined are labeled.

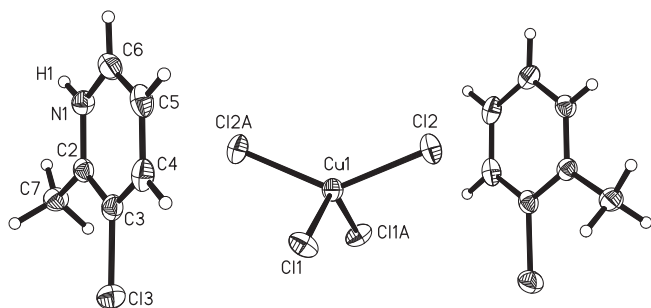


**Fig. 5.** Thermal ellipsoid plot of the molecular unit of **3** showing 50% probability ellipsoids. Only atoms in the asymmetric unit, the copper coordination plane, and hydrogen atoms whose positions were refined are labeled.

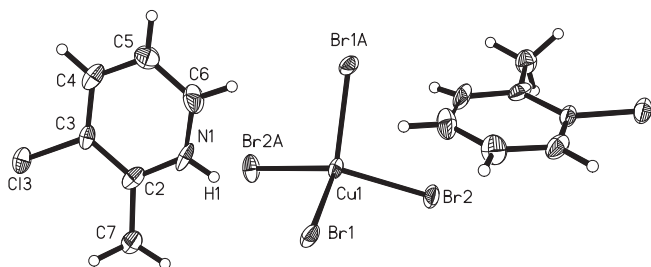


**Fig. 6.** Thermal ellipsoid plot of the molecular unit of **4** showing 50% probability ellipsoids. Only atoms in the asymmetric unit, the copper coordination plane, and hydrogen atoms whose positions were refined are labeled.

(mean dev. = 0.0025 Å). It is tilted similarly (compared to **5**) with respect to the Cu1–N1 bond ( $\angle 5.4(1)^\circ$  to the N1...C4 vector). The ring is closer to perpendicular to the Cu(II) coordination plane ( $\angle 81.0(1)^\circ$ ) than observed in **5**.

Adjacent molecular units are linked into chains by very long Cu...Br contacts ( $>4.6$  Å), suggesting that any potential magnetic superexchange via that pathway will be exceedingly weak. However, there is a second pathway which links the unit together via halide–halide contacts (Fig. 14). The Br...Br separation of 4.809(1) Å is within the range where weak magnetic exchange

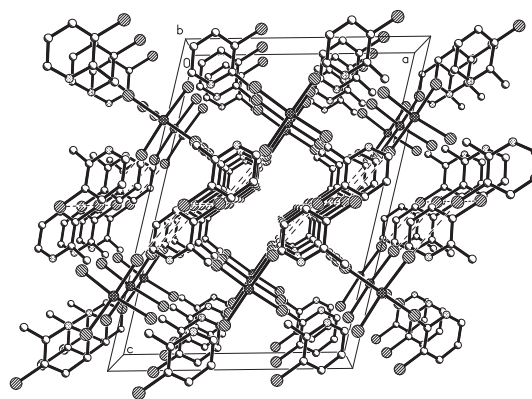


**Fig. 7.** Packing of compound **4** viewed parallel to the  $b$ -axis. Hydrogen atoms have been removed for clarity. Dashed lines show short Cl...Cl and Cl...Br contacts.

via that pathway has been observed, and the Cu1–Br1...Br1A–Cu1A torsion angle of  $180^\circ$  is optimal [1]. However, the Cu1–Br1...Br1b angles (identical to the Cu1a–Br1B...Br1 angle by symmetry), are approaching  $90^\circ$  ( $105.4(1)^\circ$ ), too small to expect significant exchange [1].

The three dimensional structure is further stabilized by weak halogen–halide contacts ( $d_{\text{Br} \dots \text{Br}} = 3.691(2)$  Å,  $\angle_{\text{C}3-\text{Br}3 \dots \text{Br}1\text{b}} = 151.8(2)^\circ$ ,  $\angle_{\text{Br}3 \dots \text{Br}1\text{b}-\text{Cu}1\text{a}} = 114.6(2)^\circ$ ).

The molecular unit of **8** is shown in Fig. 13b. The N1–Cu–Br1 angle is  $90.19(16)^\circ$ , again nearly square planar. The pyridinium ring is nearly planar (mean deviation = 0.0044 Å) and it is tilted much less with respect to the Cu1–N1 bond ( $\angle 2.7(1)^\circ$  to the N1...C4 vector) than observed in **5** or **6**. The ring is almost perpendicular to the Cu(II) coordination plane ( $\angle 84.5(1)^\circ$ ). As was the case in the bromide compound **6**, adjacent molecular units are linked into chains by very long Cu...Br contacts ( $>4.6$  Å), so any magnetic superexchange via that pathway is expected to be weak. Similar to **6**, there is a potential bromide...bromide overlap pathway (as in Fig. 14). Although the Br...Br separation is smaller than in **6** (4.68(1) Å), the Cu1–Br1...Br1b angle ( $105.4^\circ$ ) is again close to  $90^\circ$  and significant exchange is not expected [1]. The three dimensional structure is again stabilized by halogen–halide contacts ( $d_{\text{Cl} \dots \text{Br}} = 3.739(2)$ ,  $\angle_{\text{C}3-\text{Cl}3 \dots \text{Br}1\text{b}} = 147.3(2)^\circ$ ,  $\angle_{\text{Cl}3 \dots \text{Br}1\text{b}-\text{Cu}1\text{a}} = 111.2(2)^\circ$ ).

Compound **7** is unique among the neutral complexes. The complex crystallizes in the triclinic space group  $P\bar{1}$  with two molecules in the unit cell, situated across a crystallographic inversion center and forming dimers (Fig. 15). Each Cu(II) ion is nearly square pyramidal based on the Continuous Symmetry Measure with values of  $S_{\text{C}4\text{v}} = 0.49$  (square pyramidal) compared to  $S_{\text{D}3\text{h}} = 5.71$  (trigonal bipyramidal) [16]. The Cu(II) ion sits 0.125(8) Å above the mean coordination plane. The *trans* N and Cl angles about the copper ion are both  $\sim 171^\circ$  (Table 2). The chloride bridges provide an axial/equatorial link between the Cu ions and the Cu–Cl bond lengths are 2.31(1) and 2.73(1) Å for the equatorial and axial positions, respectively. The pyridinium rings are planar with deviations from the mean plane of 0.0066 and 0.0070 Å, for the N1 and N11 rings, respectively, and nearly coplanar with only a  $9.1(1)^\circ$  angle between them. The dimers stack parallel to the  $b$ -axis (Fig. 16).

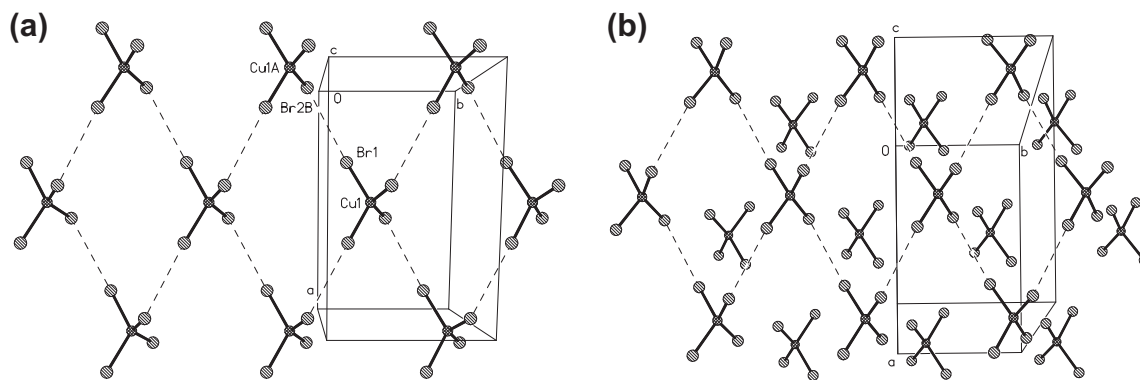


**Fig. 8.** (a) One layer of  $\text{CuBr}_4^{2-}$  ions in **4**. (b) Two layers of  $\text{CuBr}_4^{2-}$  ions in **4** viewed perpendicular to the layers showing the offset of adjacent layers.  $\text{CuBr}_4^{2-}$  ions in top layer are linked by dashed lines showing the short  $\text{Br} \cdots \text{Br}$  contacts.

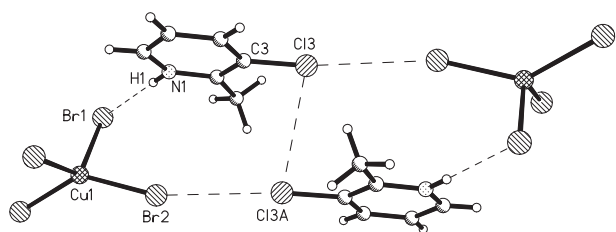


**Fig. 9.** Hydrogen bonds and short contacts between chlorine atoms and bromide ions in **4**.

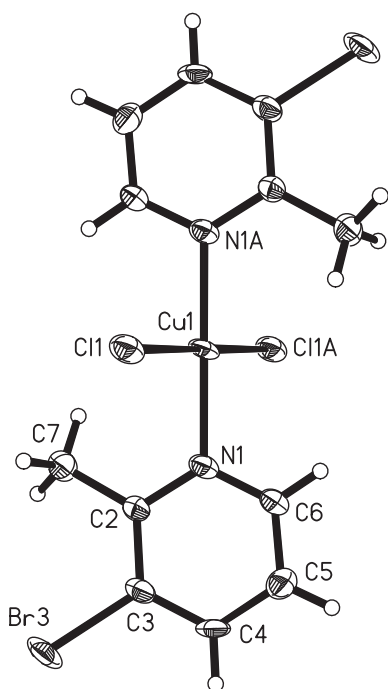


**Fig. 10.** Thermal ellipsoid plot of the molecular unit of **5** showing 50% probability ellipsoids. Only atoms in the asymmetric unit and the copper coordination plane are labeled.

The closest  $\text{Cu} \cdots \text{Cl}$  contact between dimers along the  $b$ -axis is greater than  $5.6 \text{ \AA}$  while the closest  $\text{Cl} \cdots \text{Cl}$  contacts between Cl1 and/or Cl2 ions is greater than  $8.8 \text{ \AA}$  indicating that the dimers should be very well isolated magnetically. There are short contacts between the chlorine atoms on the pyridine rings ( $d_{\text{Cl3}-\text{Cl13}} = 3.65(1) \text{ \AA}$ ) and between the chlorine atoms and chloride ions ( $d \sim 3.7\text{--}4.0 \text{ \AA}$ ) that stabilize the 3D structure (Fig. 17).

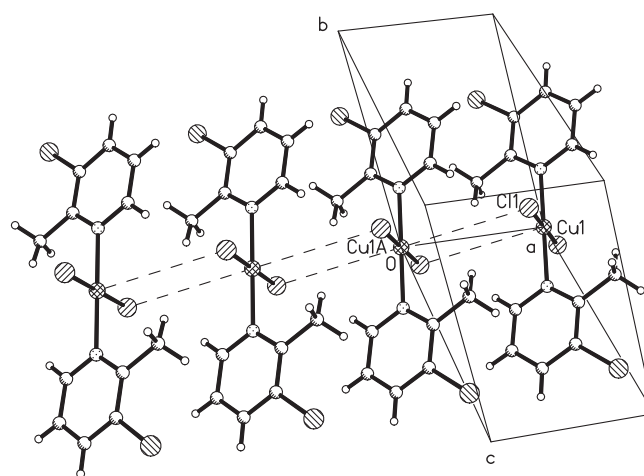


**Fig. 11.** Chain formation by intermolecular  $\text{Cu} \cdots \text{X}$  contacts in **5**.

**Table 5**  
Copper–halide contacts for compounds **5–8**.

Compound	$d_{\text{Cu1} \cdots \text{X1B}} (\text{\AA})$	$\angle_{\text{Cu1-X1} \cdots \text{Cu1A}} (^\circ)$
<b>5</b>	4.303	92.8
<b>6</b>	4.634	96.6
<b>7</b>	2.727	92.4
<b>8</b>	4.692	98.1

### 3.4. Magnetic studies

Susceptibility data were collected for compounds **1–8** from 1.8 to 310 K in a 0.1 T field. The data for compounds **1, 2, 3, 6** and **8** were fit to models for the  $S = 1/2$  uniform antiferromagnetic chain using the Hamiltonian  $\hat{H} = -\sum_{A,B} J_{AB} \hat{S}_A \cdot \hat{S}_B$  [17]. Data for compound **5** were fit to the  $S = 1/2$  uniform antiferromagnetic chain model with a Weiss correction. While the Weiss correction improved the quality of the fit slightly, the fitted value for  $\theta$  indicates that interchain interactions are negligible. Data for compound **4** were fit to the square 2D-Heisenberg antiferromagnetic model, while data for compound **7** were fit to the model for an isolated dimer. Results of the fittings are shown in Table 6.

The data for compound **1** are shown in Fig. 18 as a representative example for compounds **1, 2, 3, 6** and **8**. All exhibit very weak antiferromagnetic interactions. The paramagnetic impurity was fixed at 1% for fitting purposes (powder X-ray diffraction did not

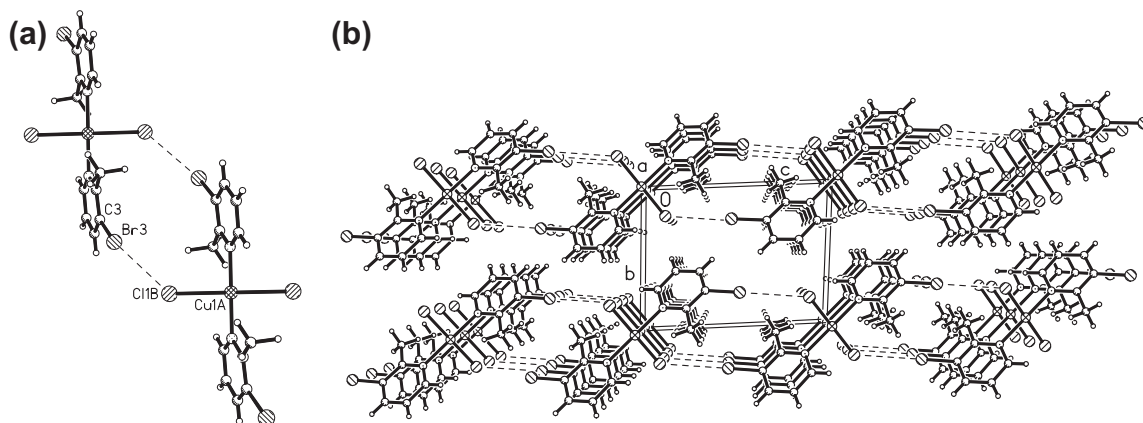


**Fig. 12.** (a) Halogen–halide contacts in 5. (b) Layer formation in 5 resulting from Cu/halide bridged chains (parallel to *a*) and halogen halide contacts (parallel to *c*).

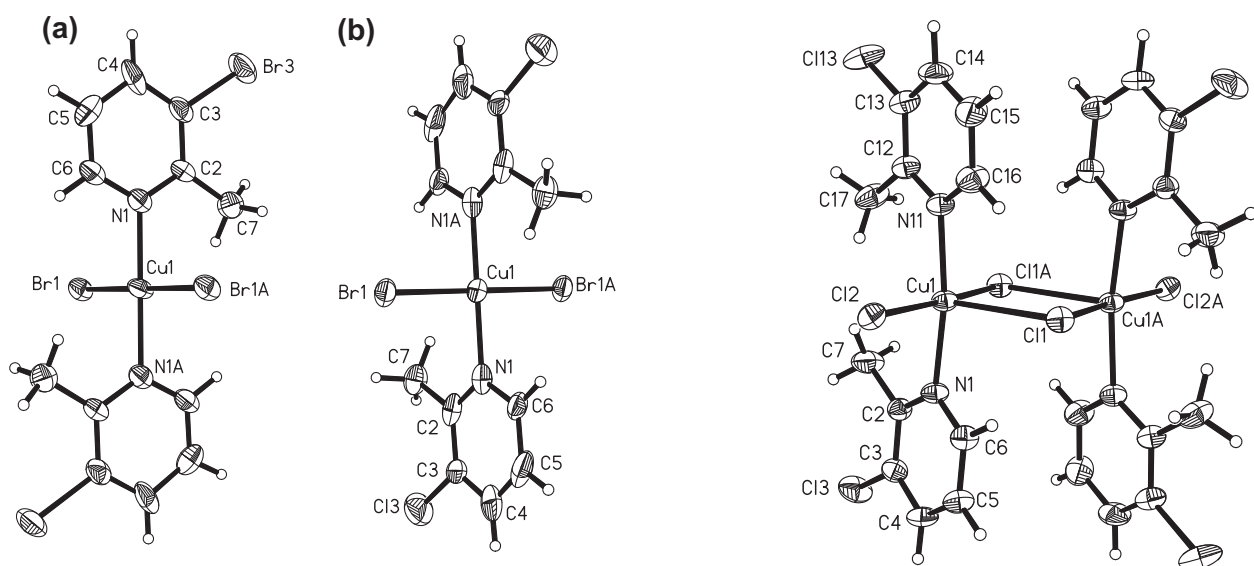


**Fig. 13.** Thermal ellipsoid plots of the molecular units of 6 (a), and 8 (b) showing 50% probability ellipsoids. Only refined atoms in the asymmetric unit and the copper coordination sphere are labeled.

**Fig. 15.** Thermal ellipsoid plot of 7 (50% probability ellipsoids) showing the dimer structure. Only atoms in the asymmetric unit and the  $\text{Cu}_2\text{Cl}_4$  moiety are labeled.

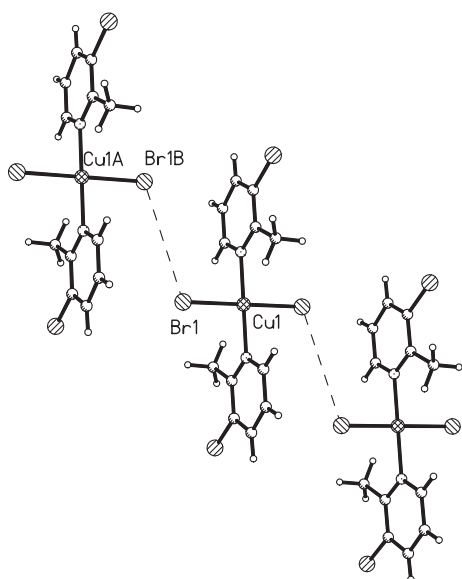


**Fig. 14.** Bromide–bromide contacts in 6.

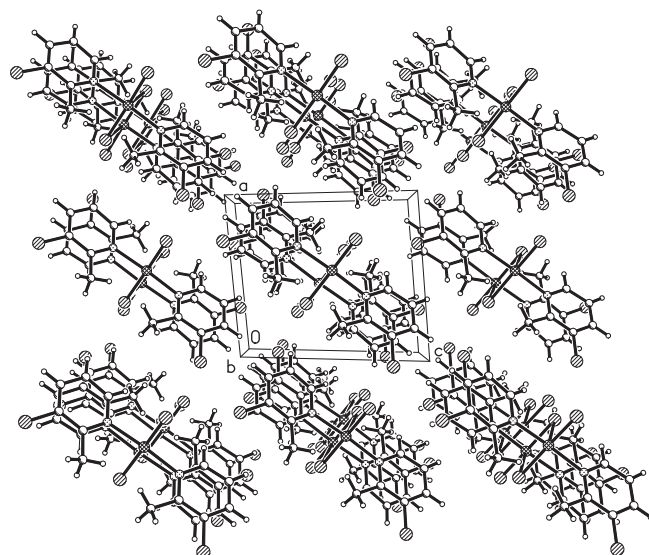


**Fig. 16.** Crystal packing of 7 viewed parallel to the *b*-axis.

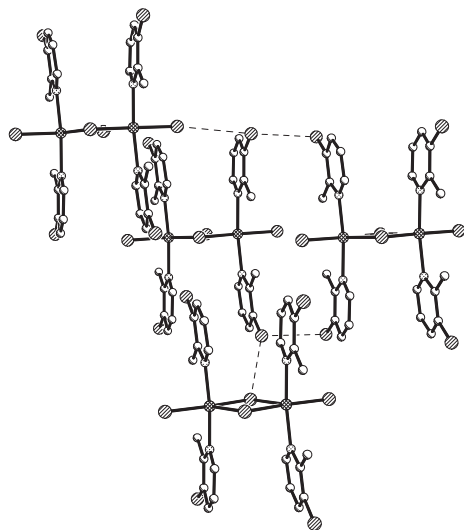


**Fig. 17.** Short chlorine–chlorine and chlorine–chloride contacts between dimers (dashed lines). Hydrogen atoms have been removed for clarity.

reveal the presence of any impurity in the sample, suggesting an upper limit for the impurity concentration). The fitted values (Table 6) show exchange values ranging from  $-0.4$  to  $-1.8$  K.

Compound **5** (Fig. 19) showed slightly stronger interactions as evidenced by the presence of a maximum in the susceptibility near 3 K.

Magnetic data for compound **4** are shown in Fig. 20. The best fit to the data was obtained using the 2D-Heisenberg model in agreement with the crystal structure. Fits obtained using a Weiss correction to account for interlayer interactions showed no change within experimental error, showing the isolation of the layers.

Data for compound **7** are given in Fig. 21. An excellent fit was obtained using the model for an isolated magnetic dimer. The quality of the fit, Curie constant, and exchange value were unchanged within experimental error when adding a Weiss correction to the model, suggesting that the dimers are very well isolated in the lattice.

#### 4. Discussion

Each of the families, salts and neutral compounds, exhibits a preferred crystal space group. The majority of the salts (compounds **1–3**), crystallize in the orthorhombic space group *Pbcn* with the  $\text{CuX}_4^{2-}$  ion located on a center of symmetry and the organic cations packing between layers of the tetrahalocuprates anions (Fig. 2a). For these complexes, however, the potential interactions between the  $\text{CuX}_4^{2-}$  within a layer are not uniform. The magnetic data are fit well by the 1D-Heisenberg uniform chain

**Table 6**  
Fitted magnetic exchange parameters for compounds **1–8**.

Compound	<i>C</i>	<i>J</i>	<i>p</i>	$\theta$
<b>1</b>	0.453(2)	$-0.415(8)$	1	
<b>2</b>	0.411(1)	$-2.35(4)$	1	
<b>3</b>	0.437(2)	$-0.437(6)$	1	
<b>4</b>	0.419(1)	$-5.09(2)$	1.07(7)	
<b>5</b>	0.419(2)	$-4.98(1)$	2.8(1)	$-0.23(4)$
<b>6</b>	0.416(2)	$-1.80(2)$	1	
<b>7</b>	0.419(1)	$-29.31(6)$	2.92(2)	
<b>8</b>	0.413(2)	$-0.612(2)$	1	

*C*, Curie constant; *J*, exchange strength.  
*p*, percent paramagnetic impurity;  $\theta$ , Weiss constant.

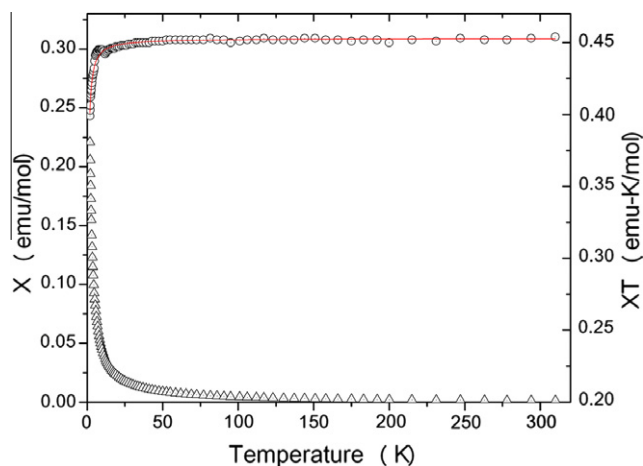


**Fig. 18.**  $\chi_m$  vs.  $T$  ( $\Delta$ ) and  $\chi_m T$  vs.  $T$  ( $\circ$ ) plots for **1** in a 1 kOe applied field. The solid line is the fit of the  $\chi T$  data to the uniform Heisenberg chain model.

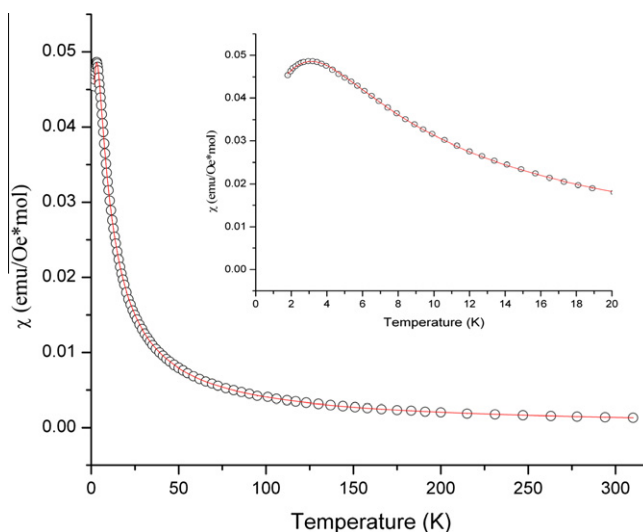


**Fig. 19.**  $\chi_m$  vs.  $T$  for compound **5** in a 1 kOe applied field. The solid line is the fit to the uniform Heisenberg chain model with a Weiss correction. The inset shows an expansion of the region from 0 to 20 K.

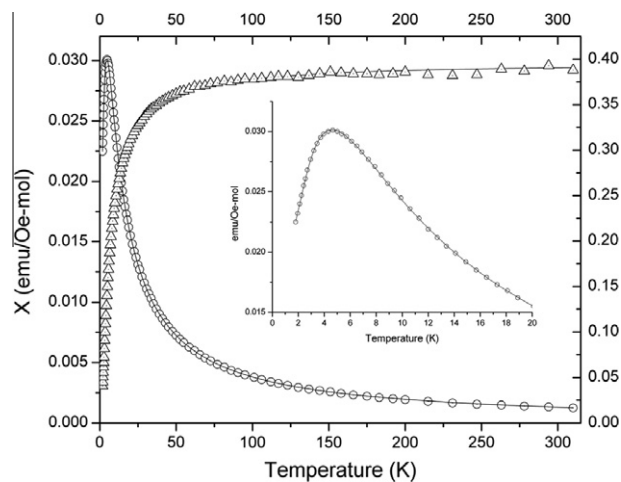


**Fig. 20.**  $\chi_m$  vs.  $T$  for compound **4** in a 1 kOe applied field. The solid line is the fit to the 2D-Heisenberg layer model. The inset shows an expansion of the region from 0 to 20 K.

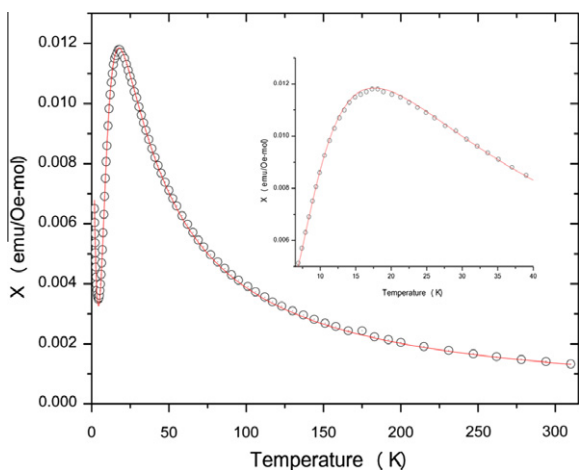


**Fig. 21.**  $\chi_m$  vs.  $T$  for compound **7**. The solid line is the fit of the data to the dimer model and includes a small paramagnetic impurity ( $\sim 3\%$ ). The inset shows an expansion of the region from 6 to 40 K.

model in agreement with the crystal structure which shows short  $X \cdots X$  contacts propagate in only one dimension. For compounds **1** and **3**, even these interactions are vanishingly weak in agreement with the large chloride  $\cdots$  chloride separation being 4.40–4.43 Å in both. The copper bromide complex, **2**, has a similar separation (4.395 Å), but the larger van der Waals radius for the bromide ion provide better orbital overlap at that distance and hence slightly stronger magnetic exchange is observed ( $-2.35(4)$  K).

The copper bromide compound **4** is unique in this group of compounds. It crystallizes in the monoclinic space group  $C2/c$ . Again, the crystal comprises layers of  $\text{CuBr}_4^{2-}$  anions with double layers of pyridinium ions separating the layers, but now the  $\text{Cu(II)}$  ions are related by the C-centering, resulting in a square magnetic lattice.  $(3\text{-Cl-2-MepyH})_2\text{CuBr}_4$  (**4**) thus becomes the newest member of a family of tetrahalocuprate complexes which generate such square layers. Other reported compounds in the family include  $(5\text{-methyl-2-aminopyridinium})_2\text{CuCl}_4$  [18],  $(5\text{-methyl-2-aminopyridinium})\text{CuBr}_4$  [18],  $(5\text{-chloro-2-aminopyridinium})_2\text{CuCl}_4$  [18],  $(5\text{-chloro-2-aminopyridinium})\text{CuBr}_4$  [18],  $(5\text{-bromo-2-aminopyridinium})_2\text{CuBr}_4$  [19] (quinolinium) $_2\text{CuBr}_4 \cdot \text{H}_2\text{O}$  [20],  $(5\text{-bromopyridinium})_2\text{CuCl}_4$  [21],  $(\text{pyridinium})_2\text{CuCl}_4$  [22]  $(4\text{-methyl-2-aminopyridinium})_2\text{CuCl}_4$  [23],  $(4\text{-aminopyridinium})_2\text{CuCl}_4$  [24],  $(4\text{-aminopyridinium})_2\text{CuBr}_4$  [25],  $(2\text{-methylimidazolium})_2\text{CuCl}_4$  [26], and  $(1\text{-methylcytosinium})_2\text{CuCl}_4$  [27]. Compounds **3** and **4**, the chloride and bromide salts respectively, are not isostructural which, while somewhat surprising, certainly has precedent having been seen previously with the  $(5\text{-bromo-2-aminopyridinium})_2\text{CuBr}_4$  [19] and  $(5\text{-bromo-2-aminopyridinium})_2\text{CuCl}_4$  [28]. In such complexes, the degree of isolation of the layers is related to the strength of magnetic interactions within and between the layers. In the present compound, the intraplane  $\text{Br} \cdots \text{Br}$  separation is 4.181 Å while the closest interplanar  $\text{Br} \cdots \text{Br}$  contact is greater than 5.6 Å. This suggests significantly better isolation than seen previously in compounds such as  $(5\text{-bromo-2-aminopyridinium})_2\text{CuBr}_4$  [19], or  $(5\text{-chloro-2-aminopyridinium})\text{CuBr}_4$  [18]. In these compounds the intraplanar separations are 4.39 and 4.35 Å respectively, both greater than the separation in **4** while the interplanar distances are 4.85 and 4.83 Å respectively, both much smaller than observed in **4**. This suggests the existence of very highly isolated layers which agrees with the fact that the 2D-Heisenberg model fits the magnetic data down to the lowest temperatures with no signs of a transition to a 3D-ordered state. The most comparably magnetically isolated tetrahalocuprate to date is the  $(\text{quinolinium})_2\text{CuBr}_4 \cdot \text{H}_2\text{O}$  [20] compound. Here the interplanar separation distance is slightly larger than in **4**

(5.74 Å), but the intraplanar distance is also greater (4.223 Å). The weaker magnetic exchange seen in **4** ( $-5.1$  K) compared to the quinolinium complex ( $-6.27$  K) demonstrates that the interhalide separation is not the only factor controlling the exchange via the two-halide pathway. Experiments at lower temperatures to locate the 3D-ordering transition in **4** are in progress.

In the neutral compounds, **5**, **6**, and **8** all crystallize in the triclinic  $P-1$  space group with the  $\text{Cu(II)}$  ion on an inversion center. Unit cell translations provide for weak  $\text{Cu} \cdots \text{X}$  contacts forming halide bibridged chains parallel to the  $a$ -axis (Fig. 11). In the bromide complexes **6** and **8** a second potential superexchange pathway is available via the two-halide pathway (Fig. 14). However, of the three only the chloride complex **5** shows significant magnetic interactions ( $J \sim -5$  K) in agreement with the large  $\text{Cu} \cdots \text{Br}$  separations ( $>4.6$  Å).

Compound **7** also crystallizes in  $P\bar{1}$ , but in this case there are two molecular units per unit cell, related by an inversion center and forming a bihalide bridged dimer (Fig. 15). The substantially shorter  $\text{Cu} \cdots \text{Cl}$  distance in the bridge ( $\sim 2.7$  Å) provides a much stronger interaction pathway and the magnetic behavior was successfully modeled as a dimer with  $J \sim -30$  K. Attempts to model the data using a Curie-Weiss correction for possible interdimer interactions did not provide a better fit, supporting the expectation of weak interactions based on the significant distances between the  $\text{Cu}_2\text{Cl}_4$  units in the crystal. A fundamental difference in local geometry is likely the cause of the difference in packing. In compounds **5**, **6**, and **8** the methyl and halogen substituents on the pyridine rings are oriented in an anti-fashion (opposite sides of the copper coordination plane), while in **7** the rings are oriented in a syn-fashion allowing sufficient room on the opposite face of the  $\text{Cu(II)}$  for two molecules to approach each other and form the dimers. This same relationship between the orientation of the ligands and the formation of chains or dimers has been reported previously for the 2-halo-3-methylpyridine complexes [8] where both orientations are observed. In addition, compounds such as  $(2\text{-methylpyridine})_2\text{CuBr}_2$  [29] and  $(2\text{-methylpyridine})_2\text{CuCl}_2$  [30] have syn-configurations for the ligands and show dimer formation, while the related complexes such as  $(\text{diethyl nicotinamide})_2\text{CuCl}_2$  [31] and  $(3\text{-}(3\text{-hydroxypropyl})\text{pyridine})_2\text{CuBr}_2$  [32], where the ligands have the anti-configuration, show the formation of bibridged chains.

Further work is in progress to identify additional materials in all categories, but especially on the layer and halide bibridged dimer complexes to try to quantify the parameters related to the magnetic superexchange and determine the relative contributions of factors such as the halide  $\cdots$  halide or halide  $\cdots$  metal distances, angles, etc. to the overall exchange. While most of these compounds show exchange that is too weak to provide highly valuable information, complexes **4** and **7** show significant interactions and will be the subject of more detailed work.

## Acknowledgments

Financial assistance from the NSF (IMR-0314773), the Kresge Foundation, and PCISynthesis toward the purchase of the MPMS SQUID magnetometer and powder diffractometer are gratefully acknowledged. M.A. is grateful for an Arthur E. Martell – Thomas T. Sugihara Summer Science Internship. The MacDiarmid Institute for Advanced Materials and Nanotechnology is thanked for funding the purchase of the Rigaku Spider X-ray diffractometer.

## Appendix A. Supplementary material

CCDC 843482, 843483, 845754, 845755, 843614, 843616, 845756 and 843615 contain the supplementary crystallographic

data for compounds **1**, **2**, **3**, **4**, **5**, **6**, **7** and **8**, respectively. These data can be obtained free of charge from The Cambridge Crystallographic Data Centre via [www.ccdc.cam.ac.uk/data\\_request/cif](http://www.ccdc.cam.ac.uk/data_request/cif). Supplementary data associated with this article can be found, in the online version, at [doi:10.1016/j.ica.2012.01.050](https://doi.org/10.1016/j.ica.2012.01.050).

## References

- [1] (a) R.D. Willett *Coord. Chem. Rev.* 109 (1991) 181; (b) M.M. Turnbull, C.P. Landee, B.M. Wells, *Coord. Chem. Rev.* 249 (2005) 2567.
- [2] (a) W.E. Estes, W.E. Hatfield, J.A.C. van Ooijen, J. Reedijk, *J. Chem. Soc., Dalton Trans.: Inorg. Chem.* 11 (1980) 2121; (b) J. Zhou, C. Ni, L. Yu, L. Yang, *Inorg. Chim. Acta* 361 (2008) 400; (c) T.J. Collins, S.W. Gordon-Wylie, E.L. Bominaar, C.P. Horwitz, G. Yee, *NATO ASI Series, Series C: Math. Phys. Sci.* 484 (1996) 509.
- [3] S.K. Hoffmann, J. Goslar, W. Hilczler, M. Krupski, L.W. ter Haar, *J. Phys.: Cond. Matt.* 11 (1999) 2437.
- [4] (a) G.W. Tremelling, B.M. Foxman, C.P. Landee, M.M. Turnbull, R.D. Willett, *Dalton Trans.* (2009) 10518; (b) K.C. Shortsleeves, L.N. Dawe, C.P. Landee, M.M. Turnbull, *Inorg. Chim. Acta* 362 (2009) 1859; (c) R. Bhattacharya, A. Ghosh, M.S. Ray, L. Righi, G. Bocelli, S. Chaudhuri, R.D. Willett, J.M. Clemente-Juan, E. Coronado, C.J. Gomez-Garcia, *Eur. J. Inorg. Chem.* (2003) 4253; (d) A. Luque, J. Sertucha, O. Castillo, P. Roman, *Polyhedron* 21 (2002) 19; (e) Antonio Luque, Jon Sertucha, Oscar Castillo, Pascual Roman, *New J. Chem.* 25 (2001) 1208.
- [5] (a) J.L. Wikaira, L. Li, R. Butcher, C.M. Fitchett, G.B. Jameson, C.P. Landee, S.G. Telfer, M.M. Turnbull, *J. Coord. Chem.* 63 (2010) 2949; (b) J.L. White, C. Lee, Ö. Günaydin-Şen, L.C. Tung, H.M. Christen, Y.J. Wang, M.M. Turnbull, C.P. Landee, R.D. McDonald, S.A. Crooker, J. Singleton, M.-H. Whangbo, J.L. Musfeldt, *Phys. Rev. B* 81 (2010) 052407; (c) A. Shapiro, C.P. Landee, M.M. Turnbull, J. Jornet, M. Deumal, J.J. Novoa, M. Robb, W. Lewis, *J. Am. Chem. Soc.* 129 (2007) 952; (d) M. Deumal, G. Giorgi, M.A. Robb, M.M. Turnbull, C.P. Landee, J.J. Novoa, *Euro. J. Inorg. Chem.* (2005) 4697; (e) F.F. Awwadi, R.D. Willett, B. Twamley, R. Schneider, C.P. Landee, *Inorg. Chem.* 47 (2008) 9327.
- [6] (a) R.T. Butcher, M.M. Turnbull, A. Shapiro, F. Xiao, C.P. Landee, D.J. Garrett, W.T. Robinson, B. Twamley, *Inorg. Chem.* 49 (2010) 427; (b) N. Tsyrlin, T. Pardini, R.R.P. Singh, F. Xiao, P. Link, A. Schneidewind, A. Hiess, C.P. Landee, M.M. Turnbull, M. Kenzelmann, *Phys. Rev. Lett.* 102 (2009) 197201; (c) R.T. Butcher, M.M. Turnbull, C.P. Landee, B.M. Wells, J.J. Novoa, J. Ribas-Ariño, A.W. Sandvik, F.F. Awwadi, *Chem. Commun.* (2009) 1359.
- [7] (a) T. Hong, S. Gvasalia, S.N. Herringer, M.M. Turnbull, C.P. Landee, L.-P. Regnault, M. Boehm, A. Zheludev, *Phys. Rev. B* 83 (2011) 052401; (b) L. Li, M.M. Turnbull, C.P. Landee, J. Jornet, M. Deumal, J.J. Wikaira, *Inorg. Chem.* 46 (2007) 11254.
- [8] S.N. Herringer, M.M. Turnbull, C.P. Landee, J.L. Wikaira, *Dalton Trans.* 40 (2011) 4242.
- [9] G.M. Sheldrick, *SHELXTL: v. 5.10, Structure Determination Software Suite*, Bruker AXS Inc., Madison, WI, 2001.
- [10] Rigaku, *CRYSTALCLEAR*, Version 1.4.0, Rigaku Americas Corporation, The Woodlands, Texas, USA, 2005.
- [11] Rigaku, *PROCESS-AUTO*, Rigaku Corporation, Tokyo, Japan, 1998.
- [12] G.M. Sheldrick, *Acta Crystallogr., Sect. A: Found. Crystallogr.* 64 (2008) 112.
- [13] Richard L. Carlin, *Magnetochemistry*, Springer-Verlag, Berlin, 1986.
- [14] R.D. Willett, *Coord. Chem. Rev.* 109 (1991) 181.
- [15] (a) F.F. Awwadi, R.D. Willett, B. Twamley, *Cryst. Growth Des.* 7 (2007) 624; (b) F.F. Awwadi, R.D. Willett, S.F. Haddad, B. Twamley, *Cryst. Growth Des.* 2006 (1833) 6.
- [16] (a) M. Pinsky, D. Avnir, *Inorg. Chem.* 37 (1998) 5575; (b) B.R. Landry, M.M. Turnbull, *J. Chem. Crystallogr.* 37 (2007) 81.
- [17] D.C. Johnston, R.K. Kremer, M. Troyer, X. Wang, A. Klumper, S.L. Bud'ko, A.F. Panchula, P.C. Canfield, *Phys. Rev. B* 61 (2000) 9558.
- [18] F.M. Woodward, A.S. Albrecht, C.M. Wynn, C.P. Landee, M.M. Turnbull, *Phys. Rev. B* 65 (2002) 144412.
- [19] F.M. Woodward, C.P. Landee, J. Giantsidis, M.M. Turnbull, C. Richardson, *Inorg. Chim. Acta* 324 (2001) 324.
- [20] R.T. Butcher, M.M. Turnbull, A. Shapiro, F. Xiao, C.P. Landee, D.J. Garrett, W.T. Robinson, B. Twamley, *Inorg. Chem.* 49 (2010) 427.
- [21] R.D. Willett, F. Awwadi, R.T. Butcher, S. Haddad, B. Twamley, *Cryst. Growth Des.* 3 (2003) 301.
- [22] M. Czugler, L. Kotai, B. Sreedhar, A. Rockenbauer, I. Gacs, S. Holly, *Eur. J. Inorg. Chem.* (2002) 3298.
- [23] R.H. Al-Far, B.F. Ali, *Acta Crystallogr., Sect. E: Struct. Rep. Online* 65 (2009) m73.
- [24] K.E. Halvorson, C. Patterson, R.D. Willett, *Acta Crystallogr., Sect. B: Struct. Sci.* 46 (1990) 508.
- [25] P. Roman, J. Sertucha, A. Luque, L. Lezama, T. Rojo, *Polyhedron* 15 (1996) 1253.
- [26] O.V. Koval'chukova, K.K. Palkina, S.B. Strashnova, B.E. Zaitsev, *Koord. Khim.* 34 (2008) 837.
- [27] G. Valle, R. Ettore, V. Peruzzo, *Acta Crystallogr., Sect. C: Cryst. Struct. Commun.* 51 (1995) 2273.
- [28] J. Giantsidis, C. Landee, M.M. Turnbull, unpublished.
- [29] P. Singh, D.Y. Jeter, W.E. Hatfield, D.J. Hodgson, *Inorg. Chem.* 11 (1972) 1657.
- [30] W.E. Marsh, W.E. Hatfield, D.J. Hodgson, *Inorg. Chem.* 21 (1982) 2679.
- [31] K.D. Onan, M. Vaidis, G. Davies, M.A. El-Sayed, A. El-Toukhy, *Inorg. Chim. Acta* 81 (1984) 7.
- [32] N. Lah, I. Leban, *Struct. Chem.* 21 (2010) 263.